



**HAL**  
open science

## Open loop thermal control of exothermal chemical reactions in multifunctional heat exchangers

Sébastien Ferrouillat, Patrice Tochon, Dominique Della Valle, Hassan Peerhossaini

► **To cite this version:**

Sébastien Ferrouillat, Patrice Tochon, Dominique Della Valle, Hassan Peerhossaini. Open loop thermal control of exothermal chemical reactions in multifunctional heat exchangers. *International Journal of Heat and Mass Transfer*, 2006, 49 (15-16), pp.2479-2490. 10.1016/j.ijheatmasstransfer.2006.01.023 . hal-00205080

**HAL Id: hal-00205080**

**<https://hal.science/hal-00205080>**

Submitted on 29 Jan 2020

**HAL** is a multi-disciplinary open access archive for the deposit and dissemination of scientific research documents, whether they are published or not. The documents may come from teaching and research institutions in France or abroad, or from public or private research centers.

L'archive ouverte pluridisciplinaire **HAL**, est destinée au dépôt et à la diffusion de documents scientifiques de niveau recherche, publiés ou non, émanant des établissements d'enseignement et de recherche français ou étrangers, des laboratoires publics ou privés.



Distributed under a Creative Commons Attribution 4.0 International License

# Open loop thermal control of exothermal chemical reactions in multifunctional heat exchangers

S. Ferrouillat <sup>a</sup>, P. Tochon <sup>a</sup>, D. Della Valle <sup>b</sup>, H. Peerhossaini <sup>b,\*</sup>

<sup>a</sup> CEA GRETh, 17 avenue des Martyrs, F-38054 Grenoble Cedex 9, France

<sup>b</sup> Thermofluids, Complex Flows and Energy Group, Laboratoire de Thermocinétique, CNRS-UMR 6607 Ecole Polytechnique de l'Université de Nantes, rue Christian Pauc, BP 50609, F-44306 Nantes Cedex 3, France

This paper presents an experimental study which demonstrates the potentiality of multifunctional heat exchangers (MHE) to carry out exothermal chemical reactions by the local control of the reactive environment temperature. Two highly exothermal chemical reactions with different kinetics (instantaneous and fast) have been investigated. The MHE is found to be very efficient in extracting the heat released by the chemical reactions. Due to its large heat transfer capacity, this process allows to increase considerably inlet reactant concentrations without thermal runaway and thus to enhance both chemical reaction conversion ratio and yield. This study also shows the limitations of the multifunctional heat exchanger for exothermal and instantaneous chemical reactions.

*Keywords:* Multifunctional compact heat exchanger; Heat exchanger; Chemical reactor; Heat exchanger-reactor; Exothermal chemical reaction; Micro-mixing; Offset strip fins; Thermal control of chemical reactions

## 1. Introduction

Process intensification (PI) is a new concept which aims at fundamental improvements in process engineering. On the one hand, it aims at the reduction of the physical size of the equipment, and on the other hand, it focuses on the achievement of a given product with specified properties and quality. More recent ideas of process intensification require a substantial decrease in the three following process properties [1]: rate of equipment size to production capacity (compactness), energy consumption (moderate production), and waste (clean production).

In this sense PI encompasses all methods of conducting a process and the usage of appropriate apparatus which allow to achieve the above goals. Therefore, improvements in materials such as catalysts and chemical path are not

considered as PI. Integration of unit operations such as mixing, reaction and heat transfer in a single device is a paramount example of process intensification. If a heat exchanger is used to accomplish mixing and reaction as well as heat transfer, then it is called a “multifunctional heat exchanger” (MHE). It is clear that in this case process intensification is no longer based on pure unit operations, but involves multi-operations. The impact of this process intensification on equipment size reduction is even more dramatic, since some types of pure processes and their associate apparatus will disappear from the future plants. The result would be safer, cheaper, compact, sustainable (environmental friendly) and energy efficient equipments in the process industry.

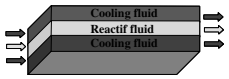
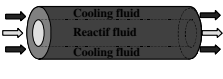
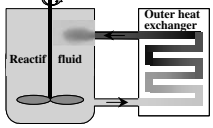
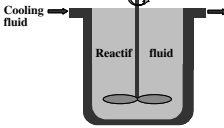
Heat transfer and fluid mechanics of the process play a crucial role in the process intensification. Some authors [2] consider the process intensification as “a design philosophy whereby the fluid dynamics in a process is matched to its chemical, biological and/or physical requirements”. Following this line of reasoning a chemical process becomes

\* Corresponding author. Tel.: +33 (0)2 40 68 31 42; fax: +33 (0)2 40 68 41 41.

*E-mail address:* hassan.peerhossaini@univ-nantes.fr (H. Peerhossaini).



Table 1  
Heat exchange capability for different reactors

Process	Compact multifunctional heat exchanger (MHE) (a)	Tubular exchanger reactor (b)	Batch reactor with outer heat exchanger (b)	Batch reactor with double envelope (b)
Scheme				
Specific area ( $\text{m}^2/\text{m}^3$ )	800	400	10	2.5
Heat transfer capacity ( $\text{W}/\text{m}^2 \text{K}$ )	5000	500	1000	400
Duty/volume ( $\text{kW}/\text{m}^3 \text{K}$ )	4000	200	10	1

(a) Results based on offset strip fins at  $Re = 2000$ .

(b) Trambouze and Euzen [7].

for a given flow rate, offset strip fins (OSF) need less pumping power but generate less micro-mixing than metallic foams, and have been retained for the present study.

In this paper, it is shown that the heat extraction capability of the MHE is suitable for temperature limitation in the case of two exothermal chemical reactions. The reactor used in this study is composed of three independent and superimposed channels of rectangular cross-section, where reactants circulates in the central channel and coolant fluids in both side channels as is shown in Fig. 1. Inside the reactive section, mixing promoters can be inserted in order to intensify mass and heat transfer. In the present study, OSF inserts were used, and their performance were compared with those of an empty duct channel (as the reference case) to highlight the gain attributable to inserts.

In order to have a modular device, the OSF inserts have not been brazed to the heat transfer surface. Indeed, with this prototype, global heat transfer coefficients reach roughly at

most  $2000 \text{ W m}^{-2} \text{ K}^{-1}$  instead of at least  $5000 \text{ W m}^{-2} \text{ K}^{-1}$  with a thermal optimized design. The thermal optimization is not addressed in this study but has been widely studied by many authors [9–11]. The available literature provides a large amount of thermal-hydraulic data on compact heat exchangers equipped or not with offset strip fins [10–13]. A short review of the two technologies selected here is given in this paper.

Two exothermal chemical reactions have been selected in order to demonstrate the MHE potentiality to control an exothermal chemical reaction: (i) an acid–base reaction between sulphuric acid ( $\text{H}_2\text{SO}_4$ ) and sodium hydroxide ( $\text{NaOH}$ ) (instantaneous), (ii) an oxidation–reduction reaction between sodium thiosulfate ( $\text{Na}_2\text{S}_2\text{O}_3$ ) and hydrogen peroxide ( $\text{H}_2\text{O}_2$ ) (fast).

This paper is organized as follows. In Section 2 the multifunctional heat exchanger is described and semi-empirical correlations used for calculation of the Nusselt number and

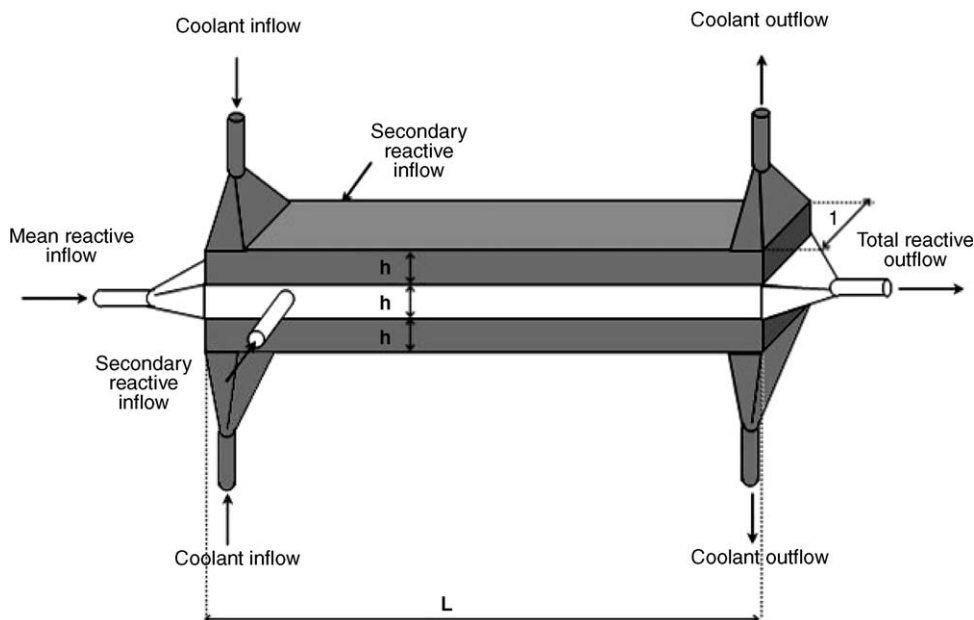


Fig. 1. Multifunctional heat exchanger.

pressure drop are presented. To facilitate the comparison of the performance of this device with similar devices now in operation, we have intentionally used the semi-empirical correlations commonly used in the industry. In Section 2 the two chemical reactions employed in the experiments are also described. Experimental results are then presented and discussed in Section 3. Section 4 summarizes the concluding remarks.

## 2. Multifunctional heat exchanger and experimental flow loop

Based on compact heat exchanger geometry, a simple and modular MHE was designed and constructed, as shown in Fig. 1. The reaction is carried out in the central rectangular channel, called the *reactive channel*. The reactive channel is surrounded by two parallel rectangular channels where coolant fluids circulate. The geometrical characteristics of the MHE are summarized as follows: height  $H = 5$  mm, width  $l = 20$  mm, length  $L = 1.47$  m, hydraulic diameter  $D_h = 8.00 \times 10^{-3}$  m, flow cross section  $S = l \times H = 1$  cm<sup>2</sup>, primary heat transfer area  $S_{\text{primary}} = 2 \times l \times L = 5.88 \times 10^{-2}$  m<sup>2</sup>, total volume  $V = L \times l \times H = 1.47 \times 10^{-4}$  m<sup>3</sup>.

For this study two geometrical configurations have been considered in the reactive central channel: an empty large aspect ratio duct channel (i.e. without inserts) and offset strip fins (OSF) usually used in compact heat exchangers.

No insert has been placed in the “double jacket” channel. This design is not thermally optimized but this could easily be done by fixing inserts in the coolant flows and brazing the fins on the support.

Fourteen “K” type thermocouples of 0.5 mm bead size have been inserted every 11 cm in the core of the reactive

channel, and four other thermocouples of the same type have been placed at the inlet and outlet of the two coolant channels to evaluate the heat balance. Temperatures are quasi uniform in the duct cross-section, as shown by DTS analysis. Therefore, for the global analysis (which is the aim of this work) one thermocouple can give a signal sufficiently representative of the bulk temperature. These temperatures are recorded on a computer through a data acquisition system. In Fig. 2 a schematic diagram of the experimental flow loop in which the MHEs have been tested. More details on the design of the loop can be found in [8]. The two reactants are stored in 50 l tanks at controlled temperature of 25 °C, and then pumped to the MHE where they are mixed.

Design rules for the two selected geometrical configurations, e.g. offset strip fins and empty duct channel, are presented in the following sections.

### 2.1. Finless duct channel

Many thermal-hydraulic correlations on empty (finless) duct channel are reported in the available literature [12,13]. A short review of pressure drop and heat transfer coefficient correlations is given here.

For a straight rectangular cross-section channel, the following correlations allow to estimate the Darcy friction coefficient. For  $Re \leq 2300$  Shah and Bhatti [14] proposed for  $0 < \alpha^* < 1$ , ( $\alpha^* = 2b/2a$ )

$$\lambda = \frac{96(1 - 1.3553\alpha^* + 1.9467\alpha^{*2} - 1.7012\alpha^{*3} + 0.9564\alpha^{*4} - 0.2537\alpha^{*5})}{Re} \quad (1)$$

where  $2b$  is the channel height (m) and  $2a$  the channel width (m).

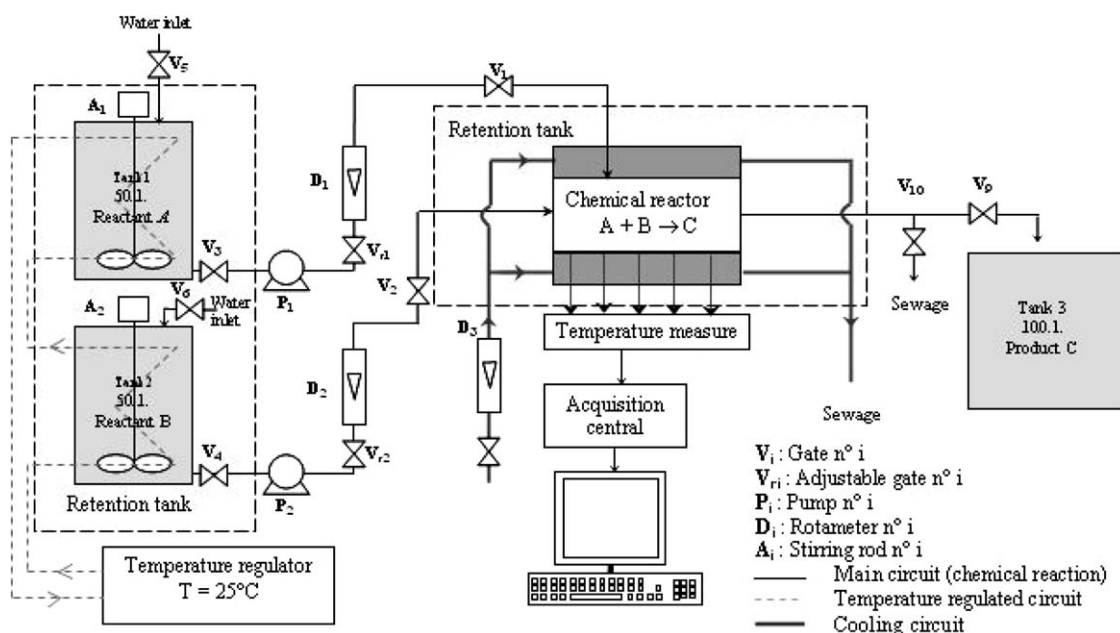


Fig. 2. Schematic diagram of the flow loop.

For  $5000 \leq Re \leq 10^7$  the same authors [14] proposed the following correlation for  $0 < \alpha^* < 1$ :

$$A = 4(1.0875 - 0.1125\alpha^*)f_c \quad (2)$$

where

$$f_c = \left( 1.7372 \ln \left( \frac{Re}{1.964 \ln Re - 3.8215} \right) \right)^{-2} \quad (3)$$

The Nusselt number in the laminar flow regime ( $0 \leq Re \leq 2300$ ) is a function of the channel aspect ratio and the thermal boundary conditions (constant wall temperature or constant wall heat flux) [14]. The relevant condition here is the constant wall heat flux. In turbulent flow regime ( $5000 \leq Re \leq 10^6$ ), the well-known Colburn correlation is used

$$Nu = 0.023Re^{0.8}Pr^{1/3} \quad (4)$$

## 2.2. Offset strip fins

### 2.2.1. Physical concepts for OSF design

In this section, the current understanding of the physics of flow and heat transfer in plate-fins heat exchangers will be described. Depending on the fins type the flow passage can be uninterrupted or interrupted, the latter being known for their high thermal efficiency. In this type, the most common geometry is the offset strip fins shown in Fig. 3. Here the fin surface is broken into a number of small sections. For each section, a new leading edge is encountered, and thus a new boundary layer starts to develop, and is then abruptly disrupted at the end of the fin offset length. The objective in such flow passages is to prevent the thickening of the boundary layers and hence provide high heat transfer coefficients. The interruptions create a wake region, and self-sustained flow unsteadiness [9]. Separation, recirculation and reattachment are the important flow features in most interrupted heat exchanger geometries. Downstream from the leading edge, the flow reattaches to the fin and

the fluid between the separating streamline and the fin surface is trapped in re-circulating zone. This region is called the *separation bubble* or *recirculation zone*. Within the recirculation zone, a relatively slow-moving fluid flows in a large eddy pattern. The boundary between the separation bubble and the separated flow (along the separation streamline) is a free-shear layer. Since free shear layers are highly unstable, velocity fluctuations develop downstream of the separation point, that are then advected downstream to the reattachment region, resulting in an increased heat transfer. The fin surface in contact with the recirculation zone is subject to lower heat transfer because of the lower fluid velocities and the thermal insulation associated with the recirculation eddy. The separation bubble increases the form drag, and thus usually represents an increase in pumping power with no corresponding gain in heat transfer. If the flow does not reattach to the surface from which it separates, a wake results. A free shear layer is also manifested in the wake region at the trailing edge of a fin element. The highly unstable wake can promote strong mixing that destroys the boundary layers from the upstream fins causing downstream heat transfer enhancement. However, at low Reynolds numbers, or for very close stream-wise spacing of fin elements, the shear layers might not be destroyed or the next fin element might be embedded in the wake of an upstream fin element. In such cases, the low velocity and near-fin temperature of the wake will have a detrimental effect on the downstream heat transfer. At low Reynolds numbers (less than 400), flow through the offset strip fin geometry is laminar and nearly steady, and the boundary layer effects dominate the heat transfer and friction. For intermediate Reynolds numbers (roughly  $400 < Re < 1000$ ), the flow remains laminar, but unsteadiness and vortex shedding become important [13,14]. For example, at  $Re = 850$ , boundary layer reconstruction causes roughly a 40% increase in heat transfer over the plain channel. Unfortunately, there is a commensurate increase in the pressure drop due to boundary layer reconstruction and vortex shedding. For Reynolds numbers greater than 1000, the flow becomes turbulent in the array, and chaotic advection may be more efficient in the low Reynolds number turbulent regime. A factor of 2 or 3 increase in heat transfer and pressure drop over plain fins can be obtained as a result of the turbulent mixing. The important variables affecting the wake region identified are the strip length, the fin spacing and the fin thickness. The fin spacing and the strip length are responsible for the boundary layer interactions and wake dissipation; and the fin thickness introduces form drag and also affects the heat transfer performance. Higher aspect ratio, shorter strip lengths and thinner fins are found to provide higher heat transfer coefficients and friction factors.

### 2.2.2. Semi empirical correlations for OSF thermal-hydraulic performance

To define the appropriate thermal-hydraulic correlations, one needs first to define the flow regime, classically

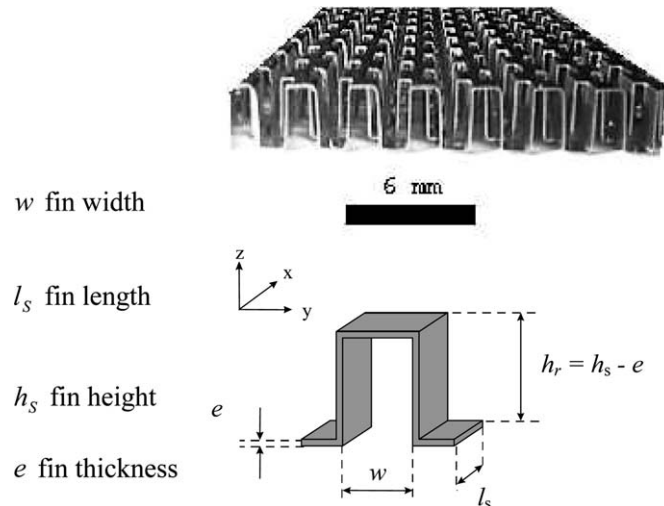


Fig. 3. Geometrical parameters of the OSF inserts.

based on the Reynolds number  $Re = (\rho U D_h)/\mu$  where  $U$  is the bulk flow velocity ( $\text{m s}^{-1}$ ),  $\rho$  the fluid density ( $\text{kg m}^{-3}$ ),  $\mu$  the fluid viscosity ( $\text{Pa s}$ ) and  $D_h$  the hydraulic diameter (m). For the OSF geometry, a photograph of the OSF inserts used in the MHE and the geometrical parameters are given in Fig. 3.

The friction factor  $f$  (fanning factor) is linked to the pressure drops  $\Delta P$  per unit length  $L$  (length of the heat exchanger) by

$$f = (\Delta P D_H) / \left[ 4L \left( \frac{1}{2} \rho U_0^2 \right) \right] \quad (5)$$

The heat transfer factor  $j$  (Colburn factor) is related to the temperature difference over the heat transfer surface by  $j = Nu_{D_H} / (Re_{D_H} Pr^{1/3})$  where the Nusselt number is defined by  $Nu_{D_H} = \frac{h D_H}{\lambda}$  and the Prandtl number  $Pr = \frac{\mu C_P}{\lambda}$ , with  $C_P$  the specific heat capacity ( $\text{J kg}^{-1} \text{ }^\circ\text{C}^{-1}$ ), and the  $\lambda$  thermal conductivity of fluid ( $\text{W m}^{-1} \text{ }^\circ\text{C}^{-1}$ ).

Correlations proposed by Manglik and Bergles [10] have been developed from the data of Kays and London, [13], in the following range of parameters:  $0.646 \leq D_H \leq 3.414$  (mm),  $0.135 \leq w/h_r \leq 1.034$  (mm),  $0.012 \leq e/l_s \leq 0.060$  (mm),  $0.038 \leq e/w \leq 0.132$  (mm).

The hydraulic diameter is defined as:

$$D_H = \frac{4w h_r l_s}{2(w l_s + h_r l_s + e h_r) + e w} \quad (6)$$

According to authors, the range of validity of these correlations is  $300 < Re_{D_H} < 10,000$ .

$$f = 9.6243 Re_{D_H}^{-0.7422} \left( \frac{w}{h_r} \right)^{-0.1856} \left( \frac{e}{l_s} \right)^{0.3053} \left( \frac{e}{w} \right)^{-0.2659} \\ \times \left[ 1 + 7.669 \times 10^{-8} Re_{D_H}^{4.429} \left( \frac{w}{h_r} \right)^{0.920} \left( \frac{e}{l_s} \right)^{3.767} \left( \frac{e}{w} \right)^{0.236} \right]^{0.1} \quad (7)$$

$$j = 0.6522 Re_{D_H}^{-0.5403} \left( \frac{w}{h_r} \right)^{-0.1541} \left( \frac{e}{l_s} \right)^{0.1499} \left( \frac{e}{w} \right)^{-0.0678} \\ \times \left[ 1 + 5.269 \times 10^{-5} Re_{D_H}^{1.340} \left( \frac{w}{h_r} \right)^{0.504} \left( \frac{e}{l_s} \right)^{0.456} \left( \frac{e}{w} \right)^{-1.055} \right]^{0.1} \quad (8)$$

Using these correlations, all the experimental results are predicted with an error less than 20%. The dimensions of the offset strip fins used in this study are summarized as follows:  $e = 0.3$  mm,  $w = 3.0$  mm,  $l_s = 1.6$  mm,  $h_s = 5.0$  mm and  $D_H = 2.0$  mm.

### 2.3. Description of the investigated chemical reactions

#### 2.3.1. Acid–base reaction

The acid–base reaction, between sulphuric acid and sodium hydroxide, is a strong acid/strong base reaction and is often considered as a total and irreversible reaction. It is instantaneous and not very temperature sensitive. All

components are miscible and flow is a single liquid phase flow. The reaction scheme is as



The reaction rate law, which is a second-order law (first-order law for each reactant), can be written as

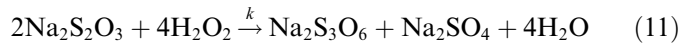
$$r = k c_{\text{H}_2\text{SO}_4} c_{\text{NaOH}} \quad (10)$$

with:  $c_{\text{H}_2\text{SO}_4}$  the sulphuric acid concentration ( $\text{mol l}^{-1}$ ),  $c_{\text{NaOH}}$  the sodium hydroxide concentration ( $\text{mol l}^{-1}$ ) and  $k = 1.4 \times 10^{11} \text{ l mol}^{-1} \text{ s}^{-1}$  at  $25^\circ\text{C}$  the reaction rate constant. The reaction enthalpy is  $\Delta H_r = -92.4$  kJ per mol of sodium hydroxide. This reaction is not very exothermic. Nevertheless, its instantaneous kinetic leads to a very local exothermicity in the process. This reaction is therefore, very useful to investigate MHE abilities in extracting a very local exothermicity.

#### 2.3.2. Oxidation–reduction reaction

The oxidation–reduction reaction between the sodium thiosulfate and the hydrogen peroxide is interesting for its demonstrative characteristic [15–17]. This reaction is irreversible, strongly exothermic and meets a fast chemical kinetics.

The reaction scheme is as follows



The reaction rate law, which is a second-order law (first-order law for each reactant), can be written as

$$r = k c_{\text{S}_2\text{O}_3^{2-}} c_{\text{H}_2\text{O}_2} \quad (12)$$

with:  $c_{\text{S}_2\text{O}_3^{2-}}$  the sodium thiosulfate concentration ( $\text{mol l}^{-1}$ ),  $c_{\text{H}_2\text{O}_2}$  the hydrogen peroxide concentration ( $\text{mol l}^{-1}$ ),  $k = k_0 \exp(E/RT)$  the reaction rate constant ( $\text{l mol}^{-1} \text{ s}^{-1}$ ),  $k_0$  the frequency factor ( $\text{l mol}^{-1} \text{ s}^{-1}$ ),  $E$  the activation energy ( $\text{J mol}^{-1}$ ),  $R = 8.314 \text{ J K}^{-1} \text{ mol}^{-1}$  the perfect gas constant,  $T$  the temperature (K).

Kinetics data available in the literature concerning this reaction are summarized as follows:  $k = 2.13 \times 10^{10} \exp(-8196/T)$  [15],  $k = 1.63 \times 10^{10} \exp(-8140/T)$  [16] and  $k = 8.13 \times 10^{11} \exp(-9156/T)$  [17]. The kinetics constant of the reaction follows an Arrhenius law and so is very sensitive to temperature. However, the hydrogen peroxide degrades at temperatures higher than  $100^\circ\text{C}$  ( $T_{\text{Boiling}} = 107^\circ\text{C}$ ). This reaction is more exothermic than the acid–base reaction. The available data on the enthalpy of this reaction are summarized as follows:  $\Delta H_r = -568$  kJ per mol of  $\text{Na}_2\text{S}_2\text{O}_3$  [15] and  $\Delta H_r = -612$  kJ per mol of  $\text{Na}_2\text{S}_2\text{O}_3$  [16].

### 3. Results and analysis

The chemical reaction evolution depends on four parameters: (i) chemical reactant concentration, (ii) micro-mixing level [18–20], (iii) reactive temperature, e.g.

global heat transfer coefficient [15–17], (iv) residence time in the process.

In order to simplify the interpretation of the results, the input conditions for chemical reactant concentrations are constant for all the runs. The three other parameters are conditioned by the process conditions, i.e. the reactive volume flow rate  $Q_{V,R}$ , and the coolant volume flow rate  $Q_{V,C}$ .

Thus, several tests have been carried out to evaluate the respective influence of the reactive and the coolant volume flow rates on the micro-mixing level, the global heat transfer coefficient and the residence time.

Test runs have been carried out with and without offset strip fins in the MHE, the empty channel being considered as the base-line configuration.

### 3.1. Acid–base reaction

For all test runs, the chemical reaction concentrations are:  $c_A = c_{H_2SO_4} = 0.5 \text{ mol l}^{-1}$  and  $c_B = c_{NaOH} = 1.0 \text{ mol l}^{-1}$ .

The sum of the volume flow rates of reactants A and B represents the total reactive volume flow rate  $Q_{V,R}$  and  $Q_A = Q_B$ . In total five series of experiments have been carried out, all tests characteristics are summarized in Table 2.

Comparison between the test cases 1 and 2 shown in Fig. 4 allows to discern the effects of coolant volume flow

rate for a MHE configuration without fins. The coolant volume flow rates are  $400 \text{ l h}^{-1}$  and  $200 \text{ l h}^{-1}$  respectively for tests 1 and 2, leading to global heat transfer coefficients of respectively  $410 \text{ W m}^{-2} \text{ K}^{-1}$  and  $370 \text{ W m}^{-2} \text{ K}^{-1}$  respectively for test 1 and test 2. As shown in Fig. 10, the reactive temperature reaches a sharp peak due to the local exothermicity and then decreases slowly along the MHE. The global heat transfer coefficient seems to have a negligible influence on the exothermal peak magnitude, but has a significant influence on the reactive temperature decrease after the peak.

Fig. 5 compares the reactive temperature rise for tests 1 and 3, showing the effect of reactive volume flow rate (Table 2 ) also carried out without fins. It shows that an increase in reactive volume flow rate at constant coolant volume flow rate leads also to an increase in the global heat transfer coefficient, but at the same time, it leads to an increase of mixing via the turbulence and a decrease in the residence time. The combined consequence of these effects is that for a given residence time, one observes a faster decrease of the temperature when the reactive volume flow rate increases from a lagrangian point of view. However, the outlet temperature of the MHE is higher for test run 3 than 1, meaning that the negative effect of the residence time reduction dominates the positive effect of the

Table 2  
Test characteristics for acid–base reaction

Test run	1	2	3	4	5
Geometric configuration	Empty duct channel	Empty duct channel	Empty duct channel	OSF	OSF
$Q_{V,R}$ ( $\text{l h}^{-1}$ )	50	50	100	50	100
$Q_{V,C}$ ( $\text{l h}^{-1}$ )	400	200	400	400	400
$h_R$ ( $\text{W m}^{-2} \text{ K}^{-1}$ )	470	470	1840	2900	5200
$h_C$ ( $\text{W m}^{-2} \text{ K}^{-1}$ )	3680	1840	3680	3680	3680
$H_g$ ( $\text{W m}^{-2} \text{ K}^{-1}$ )	410	370	1160	1500	1950
Reactive Reynolds number $Re^a$	1300	1300	2700	1160	2320

<sup>a</sup>  $Re$  is calculated with fluid properties estimated at the reactive average temperature.

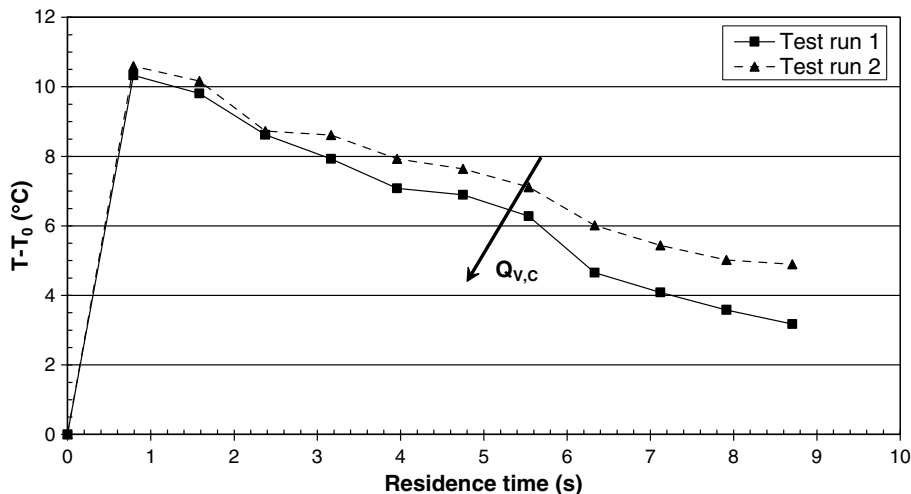


Fig. 4. Effect of coolant volume flow rate on reactive temperature rise in MHE.

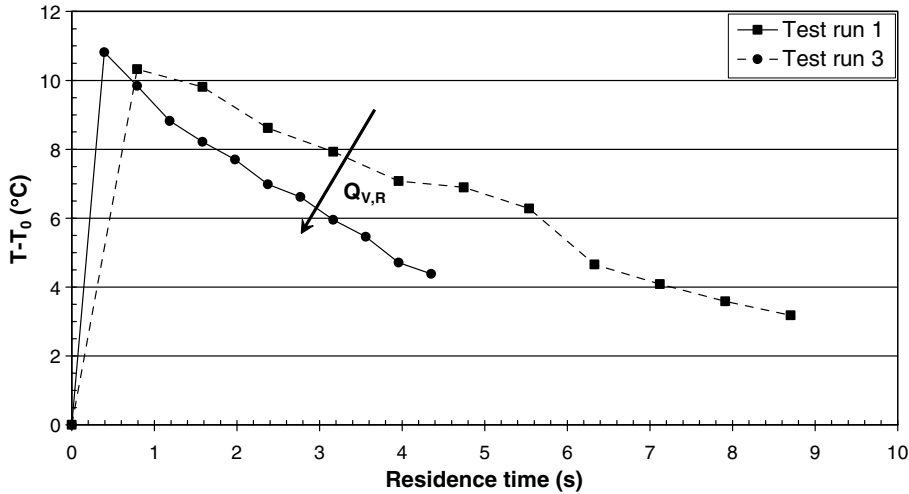


Fig. 5. Effect of coolant volume flow rate on reactive temperature rise in MHE.

flow rate. Finally, these first results show, for a reactive empty duct channel configuration, that the MHE is able to extract the heat generated by the chemical reaction.

The geometry influence on heat extraction from chemical reactions has been investigated by inserting, in the reactive channel, un-brazed offset strip fins. As shown in Table 2, for the same volume flow rate conditions, the OSF insertion leads to an increase of global heat transfer coefficient compared to empty duct channel. This heat transfer performance improvement with OSF configuration is due to interrupted flow passages which do not allow the boundary layers to thicken and thus results in high heat transfer coefficients associated with thin boundary layers. Therefore, it is logical to expect that for the same reactive flow rate and the same residence time, the OSF configuration allows to decrease significantly the reactive temperature rise compared to empty duct channel, as is shown in Fig. 6, where the temperature rise for test runs 1, 3, 4 and 5 are com-

pared. Comparison of test runs 1 and 5 shows that the outlet reactive temperatures are roughly equal while residence time is lower with the OSF configuration. In other words, for a given outlet reactive temperature, the process compactness can be improved by OSF insertion. Experiments 3 and 5 have the same reactive and the same coolant flow rates. Fig. 6 shows that the reaction temperature peak in the test run 5 (with OSFs) is lower than that of the test run 3 (empty duct channel), but has the same slope. The same observation is also valid for the results of experiments 1 and 4. It implies that the extra micro-mixing due to the OSF inserts has not increased the reaction kinetics but has provided a faster heat extraction from the reaction.

### 3.2. Oxidation–reduction reaction

Contrary to the acid–base reaction which reacts instantaneously near the reactant mixing area, this chemical reac-

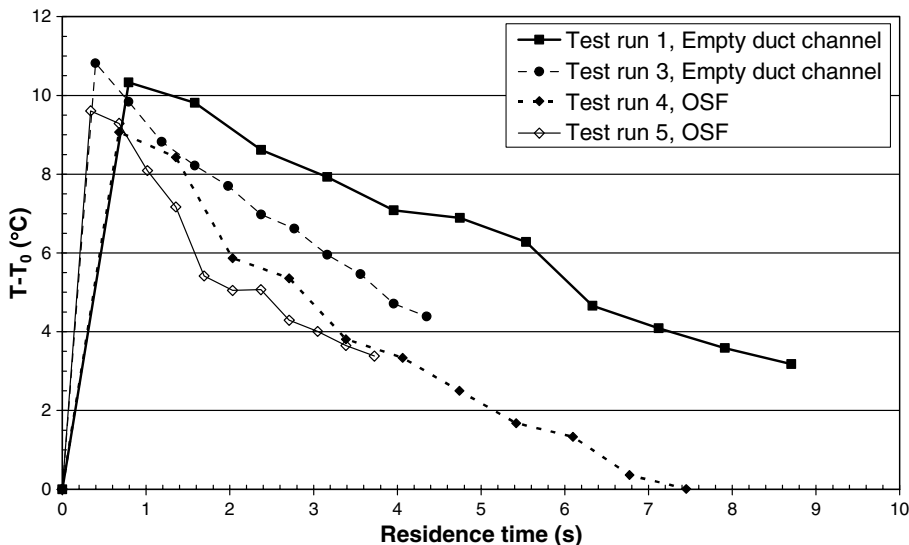


Fig. 6. Effect of the geometrical configuration on cooling of chemical reaction.

tion reacts gradually along the MHE. Moreover, the chemical reaction kinetics depends on the temperature. Thus, the chemical reaction evolution is closely linked to the micro-mixing level and the heat transfer coefficient. In order to discriminate both effects, experiments have been carried out in a first step without heat extraction, in quasi adiabatic conditions since the heat transfer takes place in a diffusive mode out of the reactor, so that micro-mixing effects are seen on chemical reaction evolution. In a second step, the global heat transfer effect on chemical reaction is investigated by the use of the active coolant flow.

For all test runs, chemical reaction concentrations are as follows:  $c_A = c_{\text{Na}_2\text{SO}_4} = 0.4 \text{ mol l}^{-1}$ ,  $c_B = c_{\text{H}_2\text{O}_2} = 0.8 \text{ mol l}^{-1}$ .

The sum of the volume flow rates of reactants A and B represents the total reactive volume flow rate  $Q_{V,R}$  where  $Q_A = Q_B$ . All test characteristics of this series of experiments are summarized in Table 3.

Without heat removal, the reactive temperature increases and this leads to an acceleration of the chemical reaction kinetics, and thus a conversion rate increase in the process outlet. Moreover, adiabatic conditions allow to compute the conversion rate at a given position in the MHE.

$$X_A(x) = \frac{T(x) - T(0)}{T_{100\%}} \quad (13)$$

with  $T(x)$  is the temperature at the position  $x$  ( $^{\circ}\text{C}$ ) and  $T_{100\%} = (\Delta H_r C_{A,0})/(\rho C_P)$  is the theoretical temperature for a 100% conversion rate ( $^{\circ}\text{C}$ ).

In these expressions, fluid properties have been estimated at the average temperature  $(T_{100\%} + T(0))/2$ . The  $T_{100\%}$  calculation is then realized by an iterative method.

Tests 5, 6 and 7 have been carried out in the “finless” channel configuration with different reactive volume flow rates (12, 25 and  $50 \text{ l h}^{-1}$ ), which correspond respectively to Reynolds numbers of 400, 670 and 1200. As shown in Fig. 7, the comparison of these three tests results show that the chemical reaction progress is roughly the same for a given residence time. Indeed, since for each test the chemical reaction kinetics is fixed by equal initial chemical reactant concentrations and since reactant mixing level is also fixed by laminar flow regime, one could assume that the global chemical reaction kinetics is equal for all tests as is observed in Fig. 7. However, it is difficult to deduce, from these results, whether the limiting factor is the chemical kinetics or the reactant mixing.

Then the influence of the reactor geometry has been tested by inserting the fins, which corresponds to tests 10 and 11 and which results are plotted in Fig. 8. The main difference between these two tests is the reactive volume flow rate which is  $12 \text{ l h}^{-1}$  for test 10 and  $25 \text{ l h}^{-1}$  for test

Table 3  
Test characteristics for oxidation–reduction reaction

Test run	5	6	7	8	9	10	11	12	13
Geometric configuration	Empty duct channel	OSF	OSF	OSF	OSF				
$Q_{V,R}$ ( $\text{l h}^{-1}$ )	12	25	50	12	12	12	25	12	12
$Q_{V,C}$ ( $\text{l h}^{-1}$ )	0	0	0	100	800	0	0	100	800
$h_R$ ( $\text{W m}^{-2} \text{K}^{-1}$ )	470	470	470	470	470	1200	2100	1200	1200
$h_C$ ( $\text{W m}^{-2} \text{K}^{-1}$ )	0	0	0	1840	5560	0	0	1840	5560
$H_g$ ( $\text{W m}^{-2} \text{K}^{-1}$ )	0	0	0	370	430	0	0	700	940
Reactive Reynolds number $Re^a$	400	670	1200	320	270	440	1000	320	270

<sup>a</sup>  $Re$  is calculated with fluid properties estimated at the reactive average temperature.

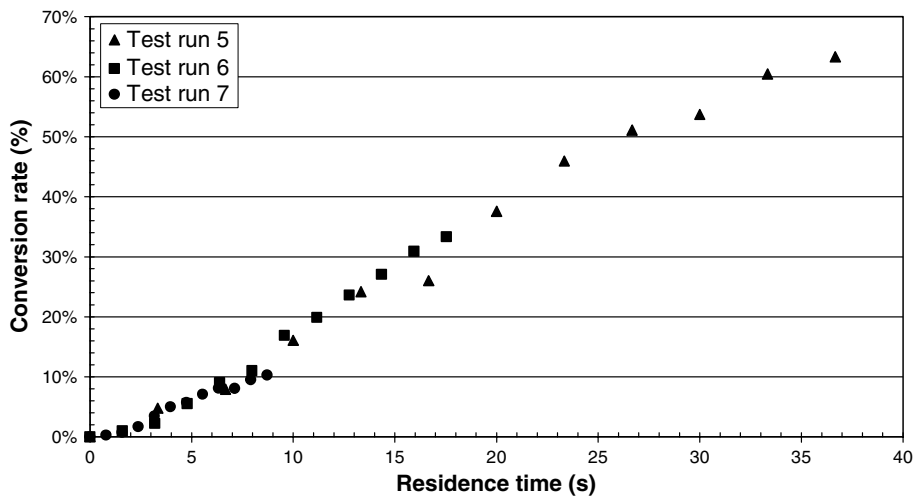


Fig. 7. Reactive conversion rate against residence time in adiabatic conditions with empty duct channel.

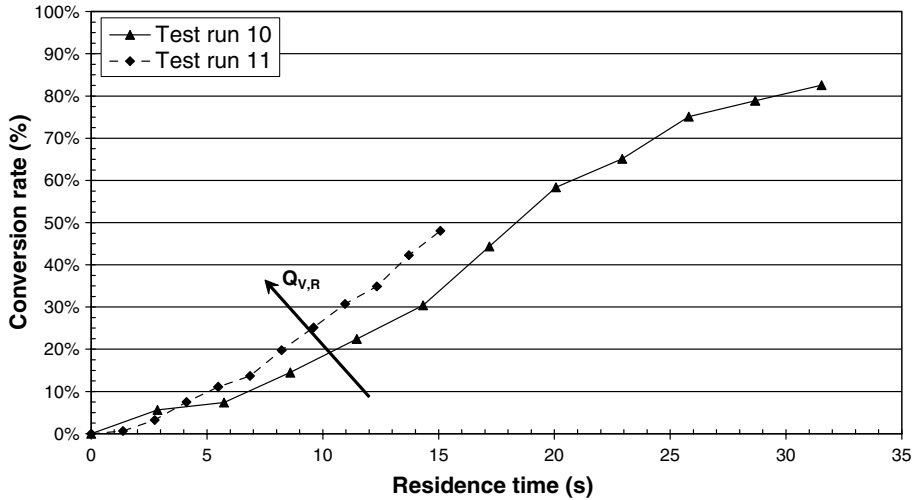


Fig. 8. Effect of reactive volume flow rate on. Reaction conversion rate with OSF.

11. This figure shows that an increase of reactive volume flow rate leads to a conversion rate increase for a given residence time. It seems thus reasonable to deduce that the global chemical reaction kinetics is controlled by reactant mixing and not by chemical reaction kinetics. This geometrical configuration allows to decrease the Reynolds number for laminar-turbulent transition by generating unsteadiness and vortex shedding downstream of the fin at  $Re = 400$  compared to the empty duct channel at  $Re = 2300$ .

It should be underlined that the chemical reaction kinetics is not constant along the process. Indeed, two different mechanism are competing: the temperature increase due to the exothermal reaction, and the decrease of the reaction rate due to the accelerated consumption of the reactants. These two effects are difficult to dissociate from these results (Fig. 8).

Chemical reaction progress also depends on the residence time. The reactive flow rate increase in the test run 11 leads to a decrease of the residence time. Thus, one could observe a lower outlet conversion rate for test run

11 than test 10. It means, as for acid-base reaction, that the negative effect of the residence time reduction dominates the positive effect of the flow rate and thus micro-mixing increase.

Finally, the two different geometrical configurations have been compared in terms of conversion rate. Fig. 9 represents the conversion rate versus residence time. Comparison of test run 6 (without fins) and test run 11 (OSF configuration) reveals that for a given residence time, conversion rate is enhanced thanks to OSF insertion which increases reactant mixing. Indeed, test run 6 is carried out at  $Re = 670$ , e.g. at laminar flow regime in empty duct channel, while test run 11 is carried out at  $Re = 1000$  where the flow becomes turbulent in the array for an OSF configuration. These results confirm that the chemical reaction progress is limited by the reactant mixing.

In order to study the global heat transfer coefficient effect on chemical reaction evolution, the reactant micro-mixing and the residence time have been fixed by equal reactant volume flow rates for all test runs. Thus, two addi-

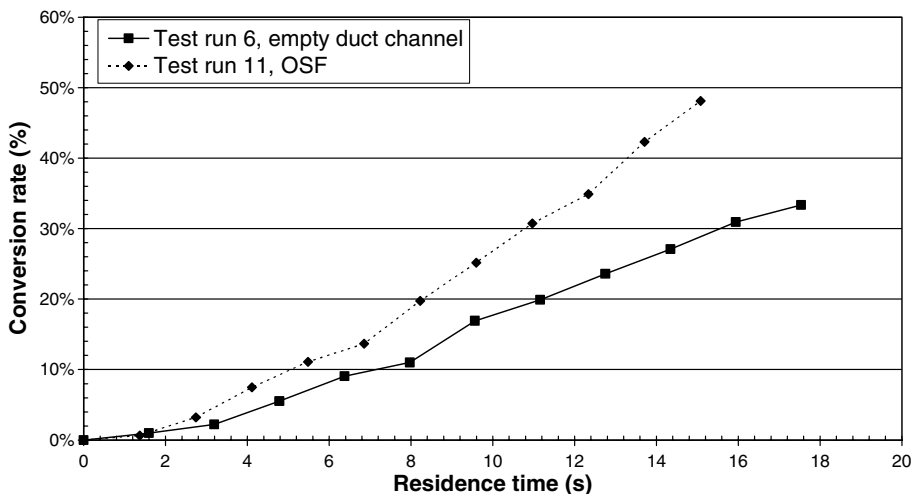


Fig. 9. Effect of geometrical configuration on reaction conversion rate.

tional tests (8 and 9) have been realized with reactive volume flow rate of  $121 \text{ h}^{-1}$  and two coolant volume flow rates (respectively  $100$  and  $800 \text{ l h}^{-1}$ ) in order to modify the global heat transfer coefficient in empty duct channel configuration. Fig. 10 shows for these tests (5, 8 and 9) reactive temperature rise versus the position in the MHE. It is discernible that the reactive temperature decreases when the global heat transfer coefficient increases. The reactive temperature decrease implies a slowing down of chemical reaction progress since the chemical reaction speed depends on, among others, temperature. Consequently, these tests also show that the MHE is able to control the chemical reaction evolution thanks to a secondary fluid flow and high level of heat transfer. Moreover, with a high global heat transfer coefficient of  $430 \text{ W m}^{-2} \text{ K}^{-1}$  in test 9, the reactive temperature is maintained at its initial temperature. In this case, the reaction has been frozen.

As for empty duct channel configuration, in order to study the global heat transfer coefficient effect of OSFs

on chemical reaction evolution, the reactant micro-mixing and the residence time have been fixed, thanks to the equal reactant volume flow rates for all tests. In addition to the adiabatic test run 10, two tests (12 and 13) have been realised with reactive volume flow rate of  $121 \text{ h}^{-1}$  and different coolant volume flow rates (respectively  $100$  and  $800 \text{ l h}^{-1}$ ) in order to modify global heat transfer coefficient via the utility side. As is shown in Table 3, for the same volume flow rate conditions, the OSF insertion increases the global heat transfer coefficient of the reactive side compared to the empty duct channel. Fig. 11 shows for the tests 10, 12 and 13 the reactive temperature versus the position in the MHE. As for empty duct channel configuration, the reactive temperature decreases when the global heat transfer coefficient increases. Even though chemical reaction progress is enhanced by reactant micro-mixing improvement due to the OSF insertion as shown previously, which leads to a higher exothermicity, the MHE is able to control the chemical reaction evolution by a secondary fluid flow.

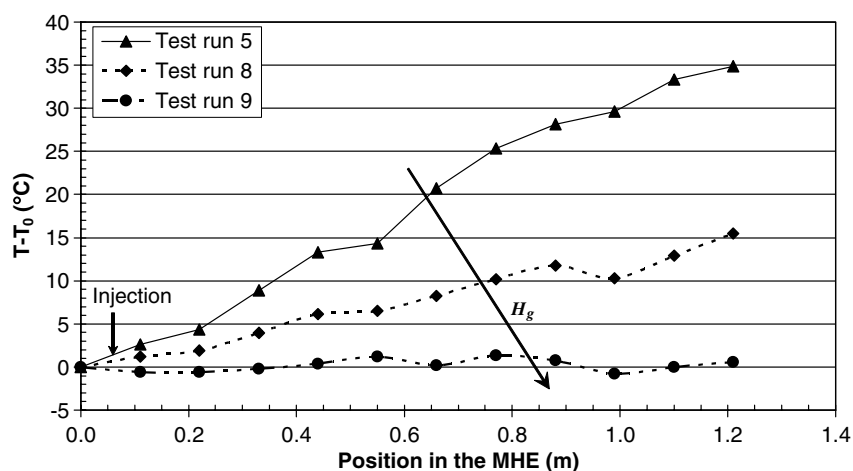


Fig. 10. Effect of heat transfer coefficient on reactive temperature rise with empty duct channel.

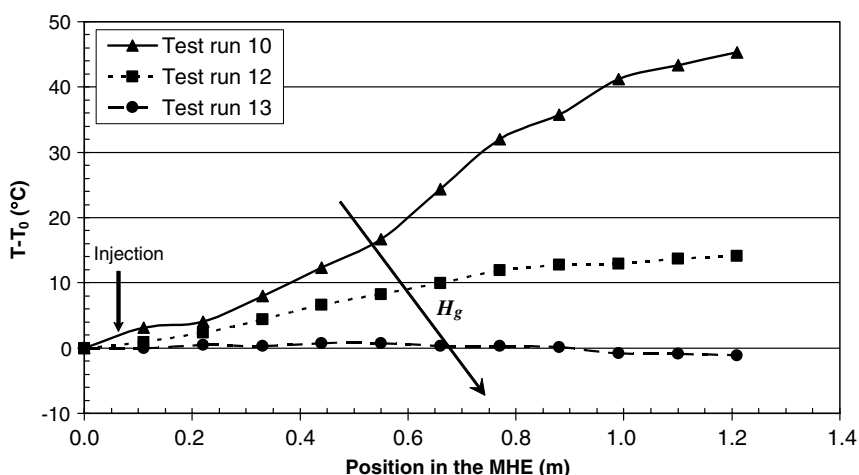


Fig. 11. Effect of heat transfer coefficient on reactive temperature in MHE with OSF inserts.

Moreover, this geometrical configuration allows to ensure at the process outlet a reactive temperature decrease of 45 °C between tests 10 and 13 compared to 35 °C between tests 5 and 9 for the simple channel configuration. With a high global convective heat transfer coefficient of  $941 \text{ W m}^{-2} \text{ K}^{-1}$  in the test 13, the reactive temperature is maintained at its initial inlet temperature.

#### 4. Conclusions

In this study, the potentiality of multifunctional heat exchangers to monitor exothermal chemical reactions through an open loop control of the reactive temperature is experimentally stated.

Actually many traditional designs such as tubular heat exchanger-reactors or classical batch reactors are often limited by their heat transfer performance for strong exothermal chemical reactions. This poor heat transfer ability forces to work with low reactant concentrations in order to avoid thermal runaway in the process.

Even without thermal optimisation (a two-fold heat transfer increase would easily be attainable with brazing), high global heat transfer coefficients can be obtained simply by adequate coolant or reactive volume flow rate. Moreover, experimental results show that OSF insertion can provide a significant mass and heat transfer intensification which lead to a considerable compactness of MHE.

Using this process allows to increase considerably inlet reactant concentrations without thermal runaway risk and consequently to enhance both chemical reaction conversion rate and yield. Nevertheless, the MHE limitations for exothermal and instantaneous chemical reactions are undeniable, since it is not able to remove instantaneously the heat generated by a very local exothermicity

As a conclusion, this work shows that heat transfer intensification is an efficient concept to improve multifunctional heat exchangers potentiality in continuous chemical engineering processes.

#### Acknowledgements

This work was partially supported by the “ENERGIE” programme of CNRS and the Ministère de la Recherche Française. S.F. acknowledges the financial support of ADEME (Agence de l’Environnement et de la Maîtrise de l’Energie) and CEA (Commissariat à l’Energie Atomique).

#### References

- [1] A.I. Stankiewicz, J.A. Moulijn, Process intensification: transforming chemical engineering, *Chem. Eng. Prog.* 1 (2000) 22–34.
- [2] V. Hessel, S. Hardt, H. Löwe, *Chemical Micro Process Engineering*, Wiley-VCH, Verlag GmbH & Co. KGaA, 2004.
- [3] J. Schütz, Agitated thin-film reactors and tubular reactors with static mixers for a rapid exothermic multiple reaction, *Chem. Eng. Sci.* 43 (8) (1988) 1975–1980.
- [4] D.W. Agar, Multifunctional reactors: old preconceptions and new dimensions, *Chem. Eng. Sci.* 54 (1999) 1299–1305.
- [5] U. Friedle, G. Verser, A counter-current heat-exchange reactor for high temperature partial oxidation reactions, *Chem. Eng. Sci.* 54 (1999) 1325–1332.
- [6] G.J. Harmsen, L.A. Chewter, Industrial applications of multifunctional multi-phase reactors, *Chem. Eng. Sci.* 54 (1999) 1541–1545.
- [7] P. Trambouze, J.P. Euzen, *Les réacteurs chimiques de la conception à la mise en œuvre*, Éditions Technip, Paris, 2002.
- [8] S. Ferrouillat, P. Tochon, H. Peerhossaini, Micromixing enhancement by turbulence: application to compact heat exchanger-reactors, *Chem. Eng. Process.*, in press.
- [9] F. Michel, P. Tochon, Ph. Marty, Simulations numériques des échanges thermiques sur une plaque épaisse, in: *Proc. Congrès français de Thermique, SFT 2002*, Vittel, 2002.
- [10] R.M. Manglik, A.E. Bergles, Heat transfer and pressure drop correlations for rectangular offset strip fins compact heat exchanger, *Exp. Thermal Fluid Sci.* 10 (1995) 171–181.
- [11] G. Xi, S. Futagami, Y. Hagiwara, K. Susuki, Flow and heat transfer characteristics of offset-fins array in the middle Reynolds number range, *ASME/JSME Thermal Eng. Proc.* 3 (1991) 151–156.
- [12] F. Michel, Optimisation des échangeurs compacts à ailettes: Étude numérique et expérimentale, PhD dissertation, University of J. Fourier, Grenoble, France, 2003.
- [13] W.M. Kays, A.L. London, *Convective Heat and Mass Transfer*, McGraw-Hill, New York, 1984.
- [14] R.K. Shah, M.S. Bhatti, *Handbook of Single Phase Convective Heat Transfer*, John Wiley & Sons, New York, 1987 (Chapters 3 and 4).
- [15] S.N. Lo, A. Cholette, Experimental study of the optimum performance of an adiabatic MT reactor, *The Can. J. Chem. Eng.* 50 (1972) 71–80.
- [16] M. Chang, R.A. Schmitz, An experimental study of oscillatory states in a stirred reactor, *Chem. Eng. Sci.* 30 (1974) 21–34.
- [17] M.D. Grau, J.M. Nougés, L. Puigjaner, Comparative study of two chemical reactions with different behaviour in batch and semi-batch reactors, *Chem. Eng. J.* 88 (2001) 225–232.
- [18] J. Villermaux, Micromixing and chemical reaction semi-quantitative criteria based on comparison of characteristic time constants, *AIChE meeting*, Chicago, paper 185a, November 1990, pp. 11–16.
- [19] J.R. Bourne, J. Baldyga, *Turbulent Mixing and Chemical Reaction*, Edition Wiley, 1999.
- [20] J. Baldyga, J.R. Bourne, A fluid approach to turbulent mixing and chemical reaction. Part I: inadequacies of available methods. Part II: micro-mixing in the light of turbulence theory. Part III: computational experimental results for the new micro-mixing model, *Chem. Eng. Commun.* 28 (1984) 231–281.